Nonisothermal Bulk Crystallization of High-Density Polyethylene via a Modified Depolarized Light Microscopy Technique: Further Analysis

Pitt Supaphol,[1] Joseph E. Spruiell[2]

[1]*Petroleum and Petrochemical College, Chulalongkorn University, Bangkok 10330, Thailand*
[2]*Materials Science and Engineering, University of Tennessee, Knoxville, Tennessee 37996*

Received 8 June 2001; accepted 4 January 2002

ABSTRACT: The quiescent nonisothermal bulk crystallization kinetics of high-density polyethylene was investigated with a modified depolarized light microscopy technique, which allowed for studies at average cooling rates of approximately 5–2500 °C min^{-1}. All of the samples crystallized at a pseudoisothermal temperature (i.e., the plateau or crystallization temperature), despite the nonisothermal nature of the cooling conditions. The rate of the crystallization process increased monotonically with increasing the cooling rate and decreasing the crystallization temperature. Moreover, the apparent crystallinity content was a certain decreasing function with the cooling rate. © 2002 Wiley Periodicals, Inc. J Appl Polym Sci 86: 1009–1022, 2002

Key words: polyethylene (PE); crystallization; kinetics (polym.)

INTRODUCTION

Studies of the nonisothermal crystallization of semicrystalline polymers have usually been carried out with differential scanning calorimetry (DSC) under modest cooling rates ranging from 1 to 80°C min^{-1}.[1] Because it is a known fact that the thermal diffusivity of all polymers is very low in comparison with that of metals and because the temperature reading shown by DSC is, in fact, that of the furnace and not that of the polymer sample itself, one cannot ignore the thermal lag occurring between the furnace and the sample, which can be significant at relatively high cooling rates (i.e., 40 $\leq$ cooling rate (T_c) $\leq$ 80°C min^{-1}). To cope with this, Janeschitz-Kriegl and coworkers[2,3] considered and used the principle of heat transfer to correct for the thermal lag occurring between the DSC furnace and the sample so that the crystallization and the kinetics of the process could be investigated with greater confidence.

Even with the correction for the thermal lag, information obtained from DSC alone may not be enough to describe the whole picture of the nonisothermal crystallization of semicrystalline polymers because a number of polymer processing techniques are normally carried out under much greater cooling rates (e.g., the cooling of melt-spun fibers and the cooling of the outer skin layer of an injection-molded article). Aiming at collecting nonisothermal crystallization kinetic data for the modeling of the melt spinning of isotactic polypropylene, Ding and Spruiell[4,5] modified the use of the depolarized light microscopy (DLM) technique, which was primarily applied to the study of isothermal crystallization by Magill[6,7] in the early 1960s, so that it could be used to study the overall nonisothermal crystallization kinetics of semicrystalline polymers under cooling conditions similar to those occurring in the melt-spinning process.

In the original DLM technique,[6,7] only the intensity of the transmitted light is recorded, the light being depolarized as a result of the formation of crystals in a sample set in a temperature-controlled hot stage between a pair of perfectly crossed polarizers. Consequently, only two quantities are of primary concern in the original technique: the transmitted depolarized light intensity and the temperature. Because a hot stage is used as a part of the setup of the original technique, studies of nonisothermal crystallization are possible, but achievable average cooling rates (ACRs) are generally less than 100°C min^{-1}.[8]

By adopting the notion of the original technique, Ding and Spruiell[4,5] extended the use of the original technique by replacing the hot stage with a specially made sample chamber in which a thin polymer sample could be heated or cooled by nitrogen gas of a controlled flow rate and temperature. The temperature of the sample is measured and recorded via a signal from a fine thermocouple embedded directly in the middle of the sample, and by adjustments in the temperature and flow rate of the cooling medium, the ACR of a thin slab of the polymer sample can be

Correspondence to: P. Supaphol (pitt.s@chula.ac.th).
Contract grant sponsor: Chulalongkorn University.

varied and controlled to about 5000°C min^{-1},[4,5,9–11] depending significantly on the design of the sample chamber and the materials used to fabricate the chamber. At such high cooling rates, however, the transmitted depolarized light intensity alone is not enough to follow nonisothermal crystallization, mainly because of the high nucleation rates encountered, which result in significant scattering of the incident light.[4,5] To cope with this, Ding and Spruiell[5] formulated a basis for the use of recorded transmitted light intensity data to correct for scattering that may be present in the transmitted depolarized light intensity data obtained. This technique is called the Ding–Spruiell technique.[4,5,12]

In this study, the nonisothermal crystallization of high-density polyethylene (HDPE) was followed and investigated with the Ding–Spruiell technique. Even though a large number of data points presented in this work were a priori published in an earlier article,[11] this article reports a number of aspects that set it apart from the earlier one. These include the following: (1) a description of the method for obtaining and treating the data at low cooling rates (<100°C min^{-1}) is provided for the first time, (2) a number of new data points collected at low cooling rates of about 5–20°C min^{-1} are included, (3) an error in computing the value of the cooling-rate factor (CRF) that appeared in the earlier article is corrected, (4) the kinetics of the nonisothermal crystallization for each cooling condition are completely reanalyzed on the basis of the Avrami macrokinetic model[13–18] with the data-fitting procedure,[19] and (5) a somewhat improved discussion of some aspects of the Ding–Spruiell technique is presented that provides insight into the merit of the technique.

THEORETICAL BACKGROUND

As mentioned previously, the uniqueness of the Ding–Spruiell technique lies in the fact that the temperature of the sample is measured and recorded via the signal from a fine thermocouple embedded directly in the sample. Because on the cooling of a sufficiently thin polymer slab the temperature distribution across the polymer sample may be assumed to be uniform, the cooling characteristics of the nonisothermal samples can be examined through heat-transfer analysis, as discussed in detail in ref. 5. This is the simplest case of the transient conduction heat-transfer problem, which involves heat conducted across the thickness from the middle of the sample to the interface between the sample and the cooling medium, at which point the heat is carried away by a convection process.[20] The heat-transfer analysis readily shows that, before crystallization, the temperature at the midpoint of the sample is given by

$$\frac{T_{s,t} - T_{cm}}{T_{s,0} - T_{cm}} = \exp\left[-\left(\frac{hb}{k}\right)\left(\frac{k}{\rho c}\frac{1}{b^2}\right)t\right] \quad (1)$$

where $T_{s,t}$, $T_{s,0}$, and T_{cm} are the temperatures of the sample at arbitrary time t, of the sample before cooling down, and of the cooling medium, respectively. h is the combinative convection heat-transfer coefficient, and k, b, ρ, and c are the thermal conductivity, half thickness, density, and heat capacity of the sample, respectively.

In addition, the term hb/k is the Biot number (Bi) physically representing the ratio of the internal thermal resistance of a solid to the boundary-layer thermal resistance. When $Bi < 1$, the temperature distribution across the surface is supposedly uniform (i.e., the temperature is independent of the position across the thickness), which is exactly the condition preferred for the Ding–Spruiell technique.[5,20] The term $k/\rho c$ is the heat diffusivity α, which designates the ability of the material to dissipate thermal energy. It should be noted that the term $kt/\rho cb$ or $\alpha t/b$ is the Fourier number (Fo) physically representing the ratio of the heat conduction rate to the rate of thermal energy storage in a solid. The rearrangement of eq. (1) results in the following equation:

$$\frac{T_{s,t} - T_{cm}}{T_{s,0} - T_{cm}} = \exp\left[-\left(\frac{h}{b\rho c}\right)t\right] \quad (2)$$

which is the form of the equation used in the original publications by Ding and Spruiell.[4,5] It is worth noting that the term $h/b\rho c$ is conveniently defined as the CRF in the original work and has a unit of the reciprocal time (i.e., s^{-1}).

In the original DLM technique, only the transmitted depolarized light intensity is recorded. It is assumed that the transmitted depolarized light intensity is linearly proportional to the development of crystallinity during crystallization of the sample, so the variation of the time-dependent relative crystallinity [$\theta(t)$] can then be computed from the following equation:

$$\theta(t) = \frac{\chi(t)}{\chi(\infty)} = \frac{I(t) - I(0)}{I(\infty) - I(0)} \quad (3)$$

where $\chi(t)$ and $\chi(\infty)$ are the absolute crystallinities at arbitrary time t and at infinite time, respectively, and $I(t)$, $I(0)$, and $I(\infty)$ are the transmitted depolarized light intensities at arbitrary time t, at time zero (i.e., before crystallization), and at infinite time (i.e., after the completion of crystallization), respectively.

The formation of crystals not only depolarizes the incident light but also scatters it. The scattering effect becomes increasingly significant with an increasing nucleation rate for crystallization at high undercoolings (under isothermal conditions) or at very high cooling rates (under nonisothermal conditions). This scattering causes the transmitted light intensity I to vary in a manner that is not directly proportional to

the crystallinity, and it can be quantified as the decrease in the transmitted light collected without an analyzer.[5] This is the main reason for the use of transmitted light intensity data recorded both with and without an analyzer to account for the structural changes during the crystallization process, as stated in the Ding–Spruiell technique. In this case, $\theta(t)$ can be instead computed from the following equation:

$$\theta(t) = \frac{\chi(t)}{\chi(\infty)} = \frac{R(t) - R(0)}{R(\infty) - R(0)} \quad (4)$$

where $R(t)$, $R(0)$, and $R(\infty)$ are the relative light intensities at arbitrary time t, at time zero (i.e., before crystallization), and at infinite time (i.e., after the completion of crystallization), respectively. Here, the relative light intensity is calculated according to the following equation:

$$R(t) = \frac{I(t) - I_c}{I_0(t)} \quad (5)$$

where $I(t)$ and $I_0(t)$ are the time-dependent transmitted light intensities collected both with and without an analyzer present in the microscope system, respectively. I_c is an empirical calibration constant that quantifies the physical characteristics of the system. A detailed description of the mathematical derivation and the performance of calibration can be found in the original publication by Ding and Spruiell.[5]

For the description of the macroscopic evolution of crystallinity during primary crystallization under quiescent, isothermal conditions, a number of macrokinetic models have been proposed over the past 60 years, including the so-called Avrami model,[13–18] the simultaneous Avrami model,[19,21] the Tobin model,[22–24] the Malkin model,[25] and the Urbanovici–Segal model.[26] Among these, the Avrami model is most widely used, partly because of its mathematical simplicity and firm theoretical basis.[27]

An analysis of the experimental $\theta(t)$ value is usually carried out in the context of the Avrami macrokinetic model:[13–18]

$$\theta(t) = 1 - \exp[-(K_a(t - t_0))^{n_a}] \in [0, 1] \quad (6)$$

where K_a is the Avrami rate constant, n_a is the Avrami exponent, and t_0 is the induction period. Normally, K_a is written in the form of the composite rate constant k_a (i.e., $k_a = K_a^{n_a}$). It should be noted that both k_a (and, therefore, K_a) and n_a are constants specific to a given crystalline morphology and type of nucleation for a particular crystallization condition,[27] and K_a has a unit of the reciprocal time (i.e., s^{-1}).

EXPERIMENTAL

Materials

The HDPE resin (labeled E12) used in this study was supplied in pellet form by Dow Chemical Co. (Baytown, Texas). The molecular weight and density information of the as-received resin was as follows: weight-average molecular weight (M_w) = 101,300 g mol^{-1}, number-average molecular weight (M_n) = 53,900 g mol^{-1}, M_w/M_n = 1.9, and ρ = 0.9540 g·cm^{-3}. The thermal properties of the as-received resin, measured with DSC at a rate of 20°C·min^{-1}, were as follows:[9] melting onset temperature (T_m^{onset}) = 127.2°C, melting peak temperature (T_m) = 132.3°C, cooling onset temperature (T_{cl}^{onset}) = 118.9°C, and cooling peak temperature (T_{cl}) = 116.7°C. The equilibrium melting temperature (T_m^0) of this resin was determined to be 142.7°C or 415.9 K.[28] To eliminate possible variations in the properties of the polymer from pellet to pellet, we cut a large number of pellets into pieces, mixed them together, and then melt-pressed them at 160°C into films.

Nonisothermal crystallization

Samples used in the Ding–Spruiell technique were prepared by portions being cut from the as-prepared film. A 25.4-μm-diameter, J-type iron/constantan thermocouple was placed between two portions of film, which were later sandwiched by a pair of clean glass slides. The whole setup was then transferred to a Mettler hot stage and was carefully pressed to give a sample of the desired thickness (ca. 80 μm) at a constant fusion temperature of 160°C. The sample was then placed in the sample chamber, which was later secured on the sample stage of a microscope. Light of controlled intensity and noise was passed through the sample and into the objective lens. The eyepieces of the binocular microscope were replaced with photocells, which were set with and without an analyzer so that transmitted light intensity data collected both with and without the analyzer were obtained.

Melting of the sample was accomplished by the passage of nitrogen gas through a separate heating unit before the connection with the sample chamber. The hot nitrogen was then blown into the chamber to heat the sample until it melted. The heating rate could be controlled by adjustments in the temperature, the flow rate of nitrogen, or both. For complete melting, the heating rate had to be slow enough and the temperature of the sample had to be brought to a certain temperature and held there for a certain period of time, depending on the polymer of interest (in this case, 160°C for at least 5 min). After this holding period, cooling of the sample was achieved by replacement of the hot nitrogen with cold nitrogen of a constant temperature. Similarly, the ACR could be con-

TABLE I
Density, Thermal Properties, and Relevant Apparent Crystallinity Content of HDPE Samples Prepared by Cooling at Different Cooling Rates

CRF (s^{-1})	ACR (°C/min)	ρ^c (g/cm^3)	T_m (°C)	ΔH_f (J/g)	$\chi_{c,DGC}$ (%)	$\chi_{c,DSC}$ (%)
0.0013[a]	10.58	0.9532	131.7	201.1	72.4	69.8
0.0024[a]	20.13	0.9528	131.6	199.2	72.1	69.2
0.0084[b]	67.83	0.9509	130.6	194.7	70.8	67.6
0.0452[b]	375.2	0.9451	129.8	176.2	66.9	61.2
0.1000[b]	794.2	0.9432	129.4	172.9	65.7	60.0
0.1441[b]	1134	0.9421	129.1	170.0	64.9	59.0
0.1257[b]	1061	0.9419	129.0	168.1	64.8	58.4
0.2038[b]	1586	0.9413	129.0	163.1	64.4	56.6
0.4154[b]	3251	0.9395	128.7	161.4	63.1	56.0
0.4418[b]	3535	0.9386	128.6	160.8	62.5	55.8

[a] Hot-stage-cooled sample.
[b] Air-cooled sample.
[c] Calculated from the position on the density gradient column according to the equation ρ (g/cm^3) = 0.0012 × Position + 0.8413.

trolled by adjustments in the temperature, the flow rate of nitrogen, or both. A personal computer was used to simultaneously record the light intensity and temperature data. A schematic illustration of the DLM setup as well as a detailed description can be found in refs. 5 and 9. This setup allowed for nonisothermal crystallization studies to be carried out under an ACR range of about 100–2500°C min^{-1} (the air-cooling regime).

To extend the use of the Ding–Spruiell technique to the study of the nonisothermal crystallization of HDPE at lower cooling rates (<100°C min^{-1}), we used a Mettler hot stage in place of the sample chamber. Even though the temperature-control module of the hot stage is sensitive enough to provide good control over the temperature settings, the temperature reflecting on the screen of the controller is in fact that of the heating elements, not that of the sample (similar to DSC). Consequently, monitoring of the temperature history of the sample was again accomplished via the signal from a thermocouple embedded directly in the sample, as described previously. Use of the Mettler hot stage as the sample chamber allowed for nonisothermal crystallization studies to be carried out under an ACR range of about 5–20°C min^{-1} (the hot stage-cooling regime).

Density, thermal properties, and apparent crystallinity content

To obtain physical information such as the density, thermal properties, and apparent crystallinity content as a function of the cooling rate, we designed and carried out a separate experiment. Ten samples were cooled at different cooling rates ranging from 10 to 3500°C min^{-1}. A combination of density gradient column (DGC) and DSC techniques was used to obtain the density, thermal properties, and apparent crystallinity content information of these samples (Table I).

The DGC used in this experiment was prepared from a mixture of isopropanol and ethylene glycol,[29] providing a density range of 0.8500–0.9700 g cm^{-3}. The density gradient along the column was carefully constructed and calibrated with five standard beads having accurately known densities until the calibration curve obtained was extremely linear. Halves of the samples prepared at different cooling rates were later put into the column and allowed to sit in the column until the positions of these samples in the column were steady. The density of each sample was then calculated from the equilibrium position according to the calibration curve obtained earlier, and the apparent crystallinity content was accordingly calculated from the value of the density obtained.

Thermal properties of the other halves of the samples were investigated with a differential scanning calorimeter (DSC-7, PerkinElmer), which was well calibrated for the temperature scale with an indium standard. The weight of each sample was kept to 3–4 mg for optimal results, and each sample was later loaded in the DSC cell, the temperature of which was preset at 50°C. The melting endotherm for each sample was recorded from 50 to 160°C at a rate of 20°C min^{-1} in an attempt to exclude the possibility of an annealing effect. The melting peak temperature and the enthalpy of fusion of each melting endotherm were recorded, and the apparent crystallinity content was accordingly calculated from the value of the enthalpy of fusion obtained.

RESULTS AND DISCUSSION

Time-dependent temperature data

Figure 1 illustrates examples of the actual cooling curves recorded for both hot-stage and air-cooling regimes. Even though all of the cooling curves in the latter regime appear to be similar to those in the

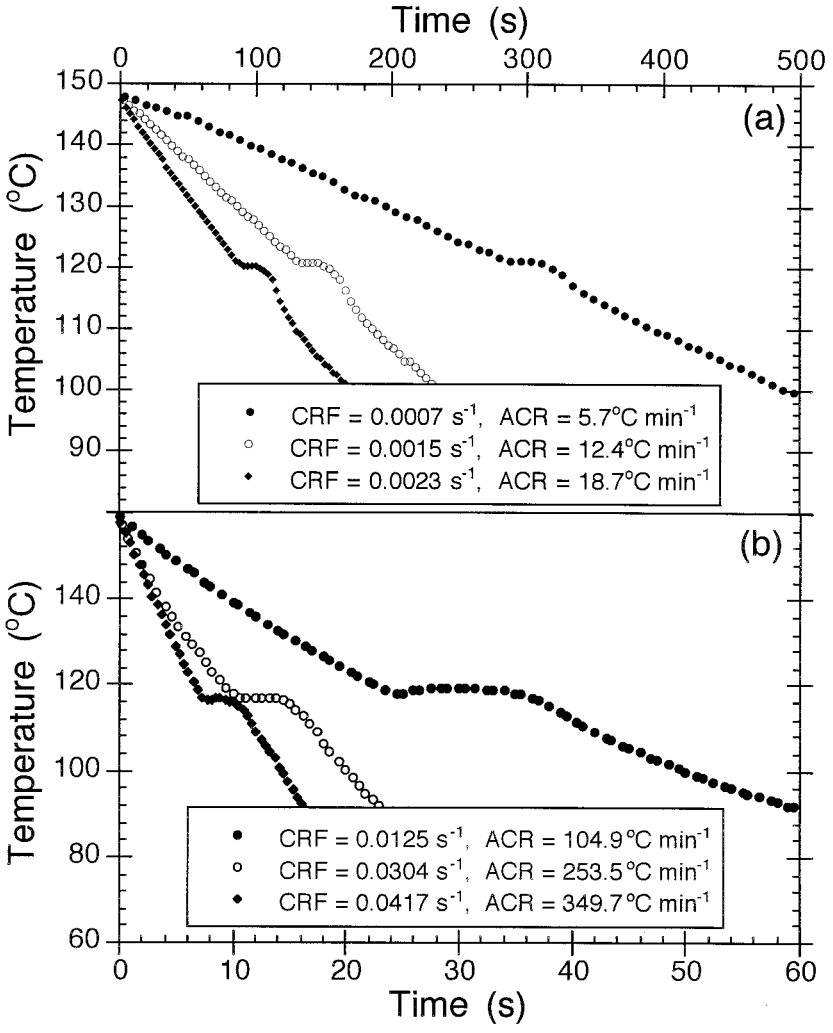

Figure 1 Actual cooling curves collected at three different cooling conditions for (a) the hot-stage-cooling regime and (b) the air-cooling regime.

hot-stage-cooling regime, the physical aspects of the cooling process between the two regimes are different. Let us first consider the cooling curves shown for the hot-stage-cooling regime [see Fig. 1(a)]. For a particular cooling curve, it is obvious that the temperature of the sample drops at a constant rate corresponding to the cooling rate preset on the Mettler controller (even though the actual cooling rate observed by the embedded thermocouple was a bit off from the preset value). The temperature continues to drop down to the point at which the crystallization process begins. It is apparent, during the crystallization, that the temperature of the sample does not follow that of the heating elements of the hot stage because of the liberated crystallization heat. This results in the formation of the plateau region (i.e., the formation of the constant-temperature region in the cooling curves). As the crystallization slows down, the temperature of the sample continues to drop and finally follows that of the heating elements of the hot stage.

Let us now turn attention to the cooling curves shown for the air-cooling regime [see Fig. 1(b)]. It is apparent that the temperature of the sample drops drastically at the very beginning of the cooling process, mainly because of the large temperature difference between the sample and the cooling medium. As for the hot-stage-cooling regime, the temperature continues to drop until the crystallization begins, during which the formation of the plateau region is also evident. After the plateau region, the crystallization process slows down significantly, even though the slow process of secondary crystallization may continue for a significant period of time. This results in a further drop in the temperature of the sample.

If the assumption of the uniform temperature profile across the thickness of the sample is valid, the temperature of the sample before the onset of crystallization (i.e., the portion before the plateau region) can be described by eq. (2). The value of CRF, which is a quantitative measure of the cooling history for a given

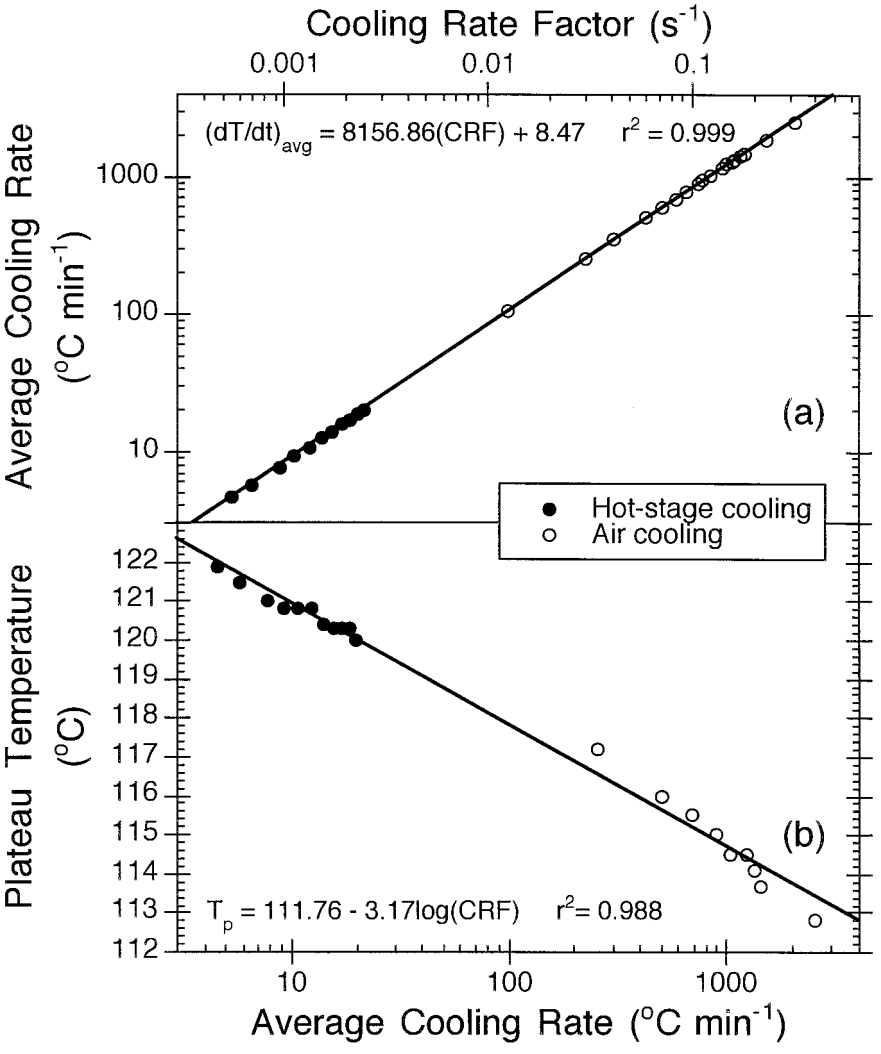

Figure 2 Relationships (a) between ACR and CRF and (b) between T_p and ACR.

cooling condition of a sample, is obtained by the direct fitting of the portion of the data before the onset of crystallization to eq. (2). A detailed description of how to determine the onset of crystallization is given later. Despite the solid physical meaning of CRF, its use to quantify the characteristics of each cooling condition is somewhat difficult to comprehend. Consequently, the use of a more familiar parameter, the ACR [$(dT/dt)_{avg}$], is an alternative to that of the CRF. The ACR can also be determined by the direct fitting of the same portion of the data to a linear equation. An illustration of the relationship between the ACR and CRF is given in Figure 2(a). According to the plot, the empirical relationship between the ACR and CRF obeys a linear relation.

As mentioned previously, the existence of the plateau region is a result of the competing contributions between the liberated crystallization heat and the heat taken away. According to Figure 1, the lowering of the position of the plateau region on the temperature axis [the plateau temperature (T_p)] with increasing ACR is evident. This phenomenon is the result of both thermodynamic and kinetic effects. Figure 2(b) illustrates the relationship between T_p and ACR.

Time-dependent transmitted light intensity data

The transmitted light intensity data collected both with and without an analyzer are illustrated in Figure 3(a) for the hot-stage-cooling regime (e.g., CRF = 0.0023 s^{-1} or ACR = 18.7°C min^{-1}) and in Figure 3(b) for the air-cooling regime (e.g., CRF = 0.0304 s^{-1} or ACR = 253.5°C min^{-1}). Obviously, the light intensity data obtained for the two regimes are similar, despite the large difference in the timescales of their experimental runs. This supports the applicability of the Ding–Spruiell technique to the study of nonisothermal crystallization over a wide range of cooling rates. Let us now consider the transmitted light intensity data shown in Figure 3 in general.

It is convenient to divide the transmitted light intensity data shown in Figure 3 into three regions. The

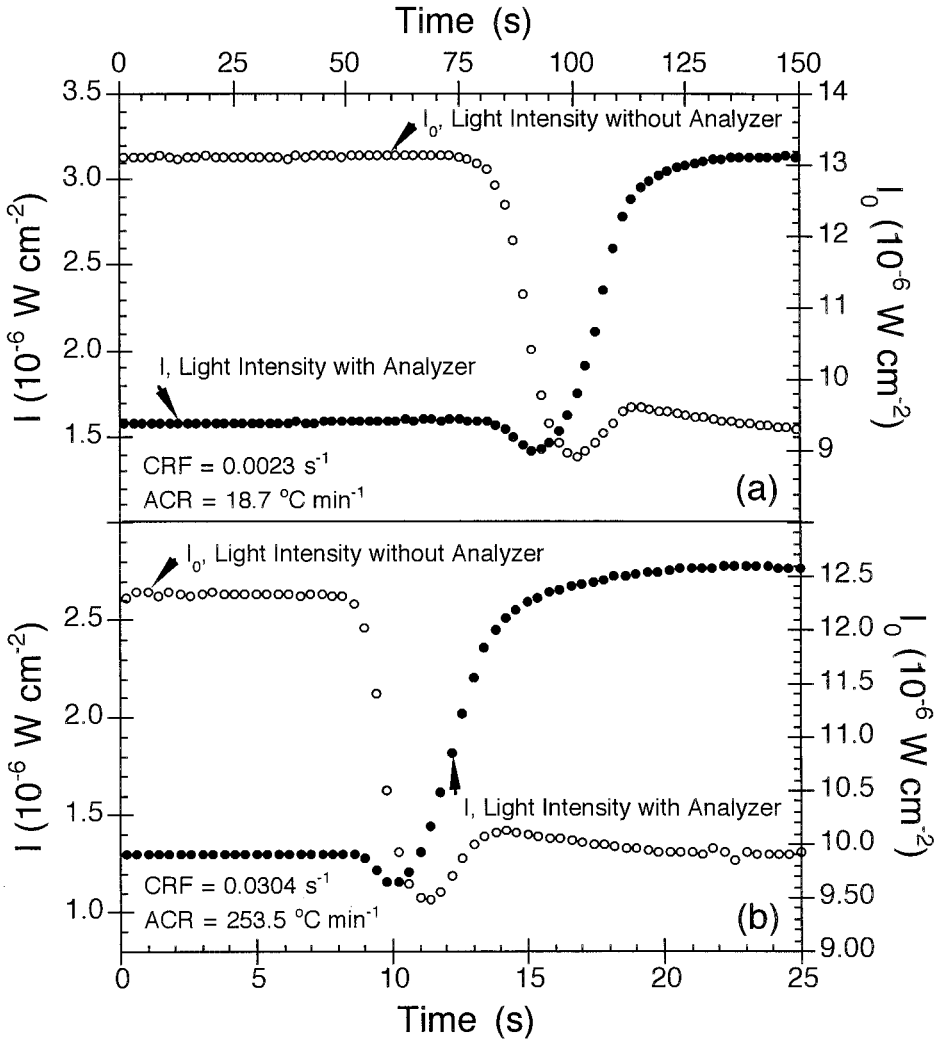

Figure 3 Overlay plots of the transmitted light intensities collected both with and without an analyzer for (a) the hot-stage-cooling regime (CRF = 0.0023 s^{-1}) and (b) the air-cooling regime (CRF = 0.0304 s^{-1}).

first region is the region in which both light intensities are constant, but it is obvious that the value of the light intensity collected with an analyzer is much lower than that of the light intensity collected without an analyzer. Because, within this region, the polymer is still in the molten state (i.e., the isotropic state), the transmitted light intensity collected without an analyzer should be at its highest value, whereas that collected with an analyzer should be at its lowest value. With ideal crossed polarizers and an isotropic sample, the transmitted light intensity collected with an analyzer should be zero. However, actual crossed polarizers have a certain level of defects that allow a certain amount of light to leak through.[5]

In the second region, as crystallization takes place, the light intensity collected without an analyzer is scattered because of the presence of small spherulites (or other crystalline aggregates), and this results in a substantial decrease in the transmitted light intensity. For the light intensity collected with an analyzer, the light scattered at the onset of crystallization causes a small dip in the transmitted light intensity. As crystallization further proceeds, the light intensity collected without an analyzer continues to drop as the growing spherulites scatter the incident light, whereas the light intensity collected with an analyzer increases in value as the growing spherulites depolarize the incident light. As these spherulites start to impinge upon one another, a smaller amount of incident light is scattered. This causes the light intensity collected without an analyzer to increase in value, reach a maximum, and finally gradually decrease and level off. In the third region, after the impingement is complete, slight changes in both light intensities may be attributed to the secondary crystallization occurring very slowly over time.

Finally, from the transmitted light intensity data collected, $\theta(t)$ can be readily computed for each cooling condition according to eqs. (4) and (5), and it is used for further analysis.

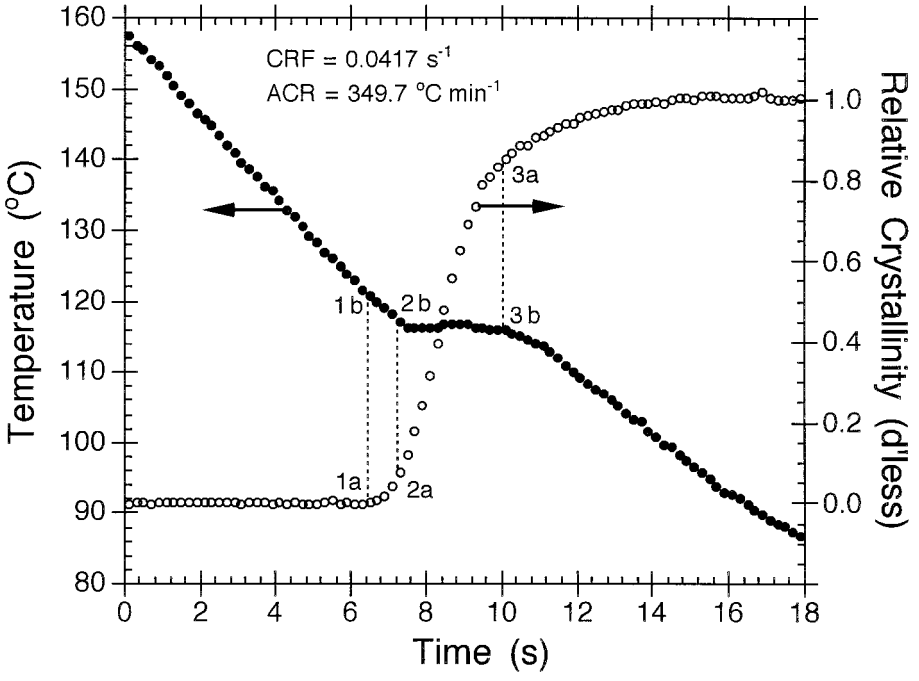

Figure 4 Overlay plots of the temperature and relative crystallinity curves for CRF = 0.0417 s^{-1}.

Formation of the plateau region

An overlay plot of the temperature and relative crystallinity curves for an air-cooled sample with CRF = 0.0417 s^{-1} or ACR = 349.7°C min^{-1} is shown in Figure 4. According to the figure, points 2b and 3b stand for the starting and ending points of the plateau region. Points 2a and 3a represent the corresponding points on the relative crystallinity curve. Here, points 1a and 1b represent the onset of the primary crystallization process on the relative crystallinity and temperature curves, respectively. To understand the formation of the plateau region, we need to establish basic knowledge about the bulk crystallization process.

It is commonly known that the crystallization process assumes a sigmoidal relationship with respect to time (see Fig. 4). Specifically, bulk crystallization can be divided into three stages. First, the early stage [ca. $0 \leq \theta(t) \leq 0.1$] is for the formation of nuclei and the subsequent growth of the nuclei into small spherulites (or other crystalline aggregates). Within this stage, the bulk crystallization rate is very slow, resulting in a very small amount of liberated crystallization heat. Second, the rapid stage [ca. $0.1 \leq \theta(t) \leq 0.7$] represents further growth of small spherulites into larger ones. This stage is thought to cease when a majority of the spherulites impinge upon one another (points 3a and 3b in Fig. 4). Within this stage, the bulk crystallization rate increases significantly as the small spherulites grow larger, reaches a maximum, and gradually decreases as impingement occurs. This stage is the stage in which the largest amount of crystallization heat is liberated. Lastly, the later stage [ca. $\theta(t) \geq 0.7$] is thought to involve the occurrence of continued secondary crystallization. Within this stage, the bulk crystallization rate gradually decreases and becomes zero at an infinite crystallization time.

According to the aforementioned mechanisms, the formation of the plateau region in the cooling curves can then be described. In the early stage of crystallization, the temperature in the plateau region continues to drop because the liberated crystallization heat cannot compensate for the amount of heat taken away by the cooling medium. As crystallization progresses further (i.e., in the rapid stage), the liberated crystallization heat increases dramatically, reaches a maximum, and finally decreases gradually. This is the reason the temperature in the plateau region often exhibits a weak maximum and finally decreases gradually. In the later stage of crystallization, the temperature in the plateau region begins to drop rapidly because the liberated crystallization heat from the secondary crystallization process is very small in comparison with the amount of heat taken away by the cooling medium. Because the majority of the crystallization process [ca. $0.1 \leq \theta(t) \leq 0.7$] occurs in the plateau region within which the temperature fluctuation is negligible, it is safe to state that even though the cooling of the samples in the Ding–Spruiell technique is nonisothermal in nature, crystallization actually occurs at a pseudoisothermal temperature. As a result, T_p is simply the crystallization temperature for a particular cooling condition.

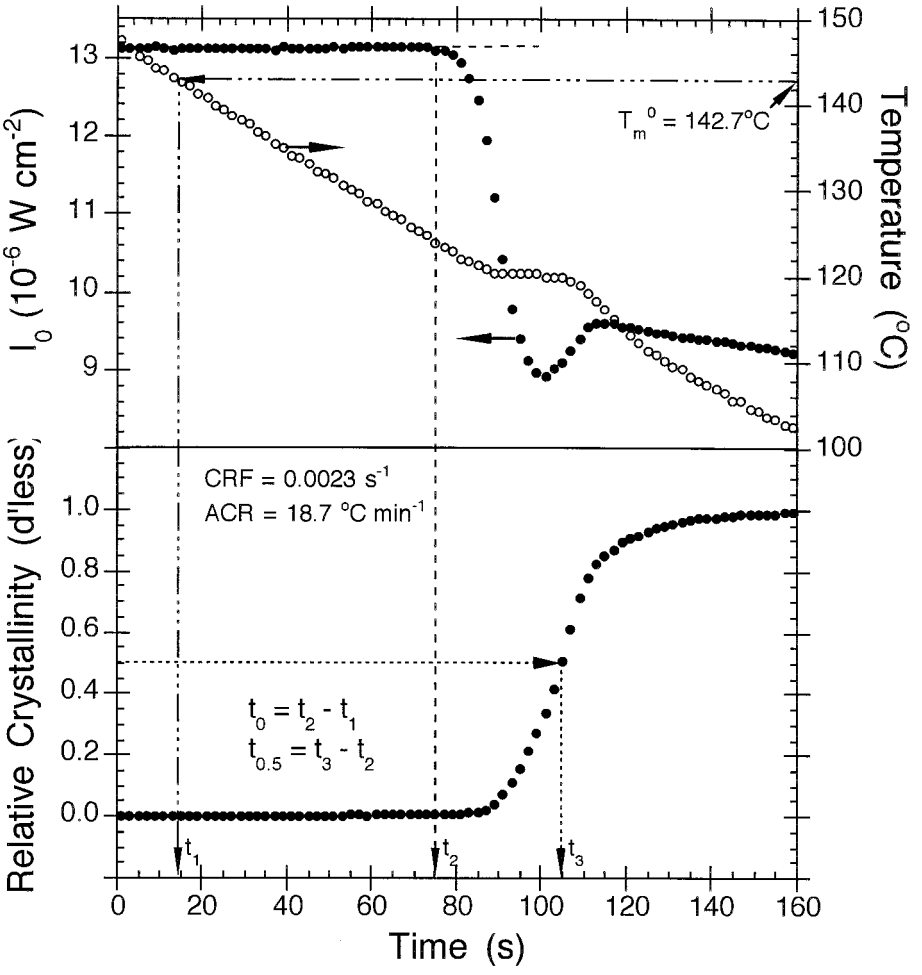

Figure 5 Schematic procedure for the determination of t_0 and $t_{0.5}$ data.

Determination of the induction time (t_0) and half-time of crystallization ($t_{0.5}$)

Let us first define the terms t_0 and $t_{0.5}$. In this article, t_0 is defined as the time interval the polymer spends from T_m^0 to the moment at which crystallization takes place, whereas $t_{0.5}$ is defined as the time interval the polymer spends from the onset of crystallization to the time at which the crystallization is half completed [i.e., at $\theta(t) = 0.5$].

To determine these two important parameters in the Ding–Spruiell technique, we require the time-dependent data of the temperature $T(t)$, the transmitted light intensity collected without an analyzer (I_0), and the relative crystallinity $\theta(t)$. These data for a hot-stage-cooled sample with CRF = 0.0023 s^{-1} or ACR = 18.7°C min^{-1} are plotted together in Figure 5 as a schematic representation of how to determine these parameters. Practically, there are four steps for determining these two parameters. First, let us consider the determination of the onset of the induction period. This is the time t_1, which is simply the projection of the T_m^0 value (i.e., for this HDPE resin, T_m^0 = 142.7°C[28]) with respect to the temperature curve onto the time axis. Second, let us consider the determination of the onset of the crystallization. This is the time t_2, which is simply the projection of the point on the light intensity curve at which the intensity data start to deviate from the common baseline onto the time axis. Third, let us consider the determination of the time at $\theta(t) = 0.5$. This is the time t_3, which is simply the projection of the point $\theta(t) = 0.5$ on the relative crystallinity curve onto the time axis. Ultimately, t_0 is calculated by the subtraction of t_1 from t_2 (i.e., $t_0 = t_2 - t_1$), whereas $t_{0.5}$ is determined by the subtraction of t_2 from t_3 (i.e., $t_{0.5} = t_3 - t_2$).

Variation of t_0 and $t_{0.5}$ with the cooling rate

t_0 and $t_{0.5}$ were found to follow a power-law relationship with the ACR. The power-law relationships of t_0 and $t_{0.5}$ with CRF can respectively be expressed as

$$t_0 = 0.156\text{CRF}^{-0.973} \quad (r^2 = 0.990) \tag{7}$$

$$t_{0.5} = 0.131\text{CRF}^{-0.887} \quad (r^2 = 0.995) \tag{8}$$

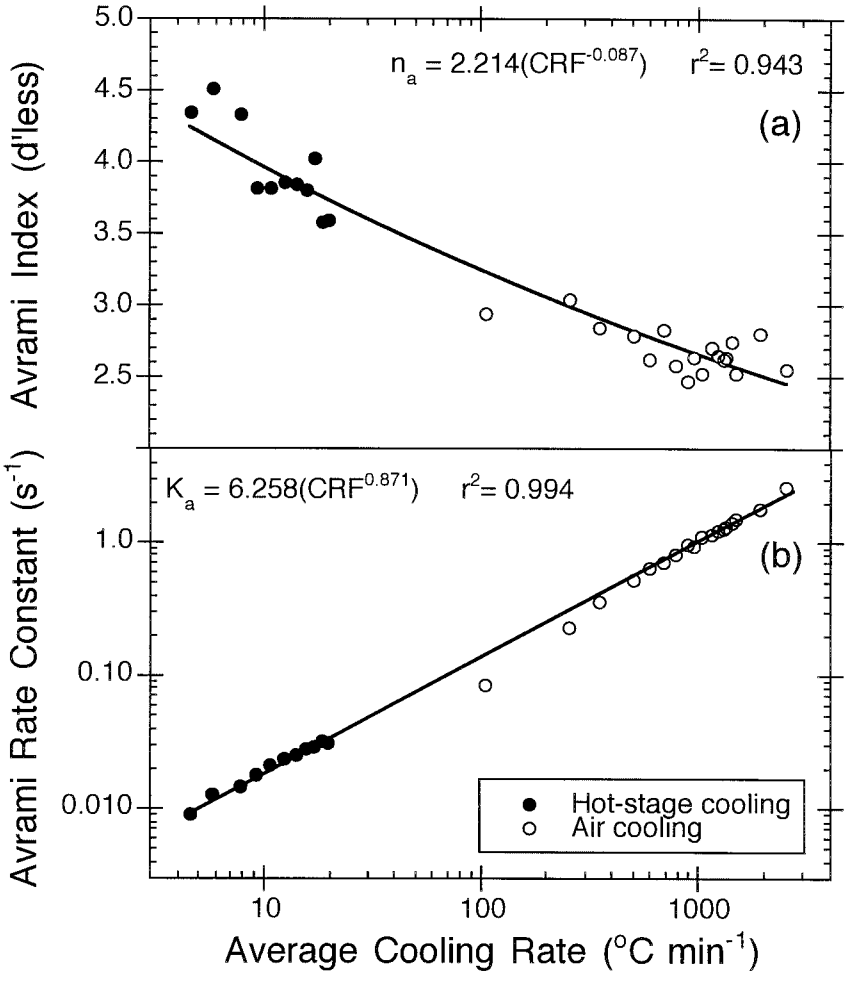

Figure 6 Relationships (a) between n_a and ACR and (b) between K_a and ACR.

Kinetics of the crystallization process

It has been stated previously that, for a particular cooling condition, a large fraction of the crystallization process takes place at a pseudoisothermal temperature (i.e., the plateau or crystallization temperature). This allows the analysis of the kinetics of the process to be carried out according to the traditional Avrami macrokinetic model [i.e., eq. (6)]. Instead of using the traditional analytical procedure mentioned previously, we can perform the data analysis with a direct data-fitting procedure[19] in which the experimental data are fitted directly to eq. (6) with a nonlinear multivariable regression program. With this analytical procedure, relevant kinetics parameters are automatically obtained along with the best fits.

Experimental results for n_a are plotted as a function of the ACR in Figure 6(a). Because n_a lies mostly between about 2.5 and 4, it can be postulated along with a direct observation under the optical microscope that the growth is three-dimensional and that the nucleation is predetermined. Figure 6(b) illustrates a log–log plot of K_a versus the ACR, in which a linear relationship between the two parameters is clearly evident. It clearly shows that K_a increases with an increasing cooling rate, suggesting that the bulk rate of crystallization increases with an increasing ACR, as expected. Interestingly, both n_a and K_a exhibit a power-law relationship with the ACR.

Temperature dependence of the crystallization rate parameters

Before going further, we should note that K_a obtained earlier is not the only parameter used to quantify the overall rate of crystallization. The reciprocal value of $t_{0.5}$ (i.e., $t_{0.5}^{-1}$) is, in fact, the most fundamental parameter used. Because these bulk rate parameters (i.e., $t_{0.5}^{-1}$ and K_a) are known to be very sensitive to changes in the temperature, a plot of such rate parameters against the crystallization temperature (i.e., T_p) is meaningful. Such a plot is illustrated in Figure 7. It is apparent that the two rate parameters exhibit a similar temperature dependence, in that both rate parameters decrease with an increasing crystallization tempera-

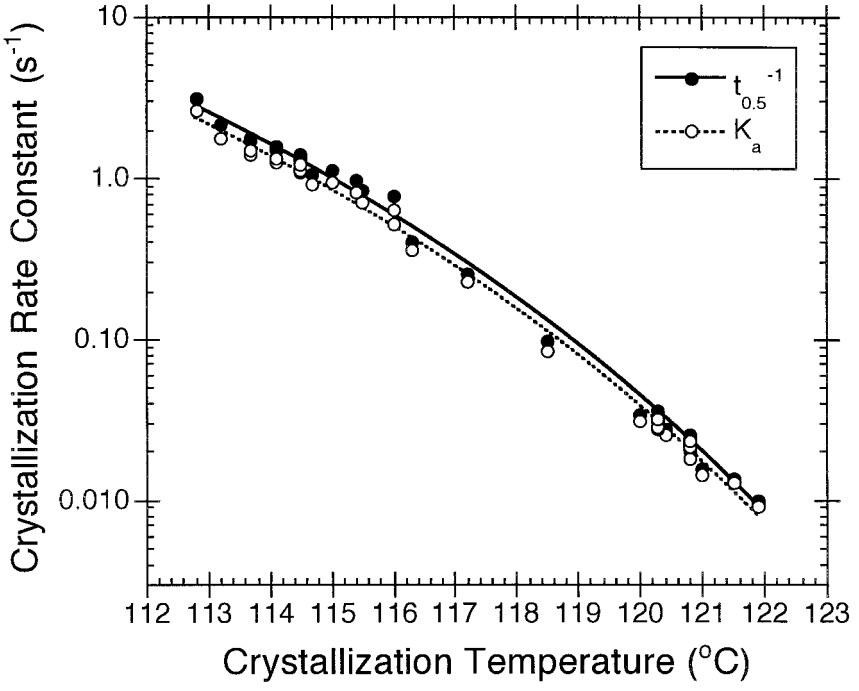

Figure 7 Relationship between the two bulk crystallization rate parameters ($t_{0.5}{}^{-1}$ and K_a) and the crystallization temperature.

ture. This similarity is quickly recognized because the two rate parameter are related to each other according to the following equation:

$$K_a = (\ln 2)^{1/n_a} \cdot t_{0.5}^{-1} \tag{9}$$

To quantify and describe the temperature dependence of the rate parameters, one has to realize that the rate parameters (i.e., $t_{0.5}{}^{-1}$ and K_a) relate, in one way or another, to the primary nucleation rate N and/or the subsequent crystal growth rate G.[30–33] Although the temperature dependencies of the parameters N and G are known to be different,[30–33] the rate parameters have often been considered to have temperature dependencies similar to that of the subsequent crystal growth rate G (written in the context of the original Lauritzen–Hoffman secondary nucleation theory,[32,33] which is given by

$$\Psi(T) = \Psi_0 \exp\left[-\frac{U^*}{R(T_c - T_\infty)} - \frac{B}{T_c(\Delta T)f}\right] \tag{10}$$

where $\Psi(T)$ and Ψ_0 are the respective rate parameter (i.e., $t_{0.5}{}^{-1}$ and K_a) and the respective pre-exponential parameter [i.e., $(t_{0.5}{}^{-1})_0$ and $K_{a,0}$], respectively. U^* is the activation energy characterizing the molecular diffusion across the melt/crystal interface (for HDPE, U^* = 6276 J mol^{-1} [32,33]), whereas B is a parameter related to the secondary nucleation. T_∞ is the characteristic temperature at which long-range molecular motion is very unlikely to occur (for HDPE, T_∞ = 160 K[34]), R is the universal gas constant, ΔT is the degree of undercooling (i.e., for this HDPE resin, $\Delta T = 415.9 - T_p$), and f is a factor used to correct for the temperature dependence of the enthalpy of fusion [i.e., for this HDPE resin, $f = 2T_p/(T_p + 415.9)$].

Finally, the temperature-dependent crystallization rate function $\Psi(T)$ can be quantified by the simple fitting of each respective rate parameter (i.e., $t_{0.5}{}^{-1}$ and K_a) to eq. (10) with the same nonlinear multivariable regression program used earlier in the Avrami analysis. The fitting parameters obtained for the results shown in Figure 7 as a solid line for $t_{0.5}{}^{-1}$ data and as a dotted line for K_a data are (1) $(t_{0.5}{}^{-1})_0 = 2.8 \times 10^8$ s^{-1} and $B = 1.7 \times 10^5$ K^2 and (2) $K_{a,0} = 2.2 \times 10^8$ s^{-1} and $B = 1.7 \times 10^5$ K^2.

Density, thermal properties, and apparent crystallinity content

The density, melting peak temperature, enthalpy of fusion, and relevant apparent crystallinity content of HDPE samples prepared by cooling at different cooling rates are reported in Figures 8 and 9. The apparent crystallinity content shown in both figures is in fact the crystallinity weight percentage calculated from the density and the enthalpy of fusion according to the following equations:

$$\chi_{c,\mathrm{DGC}}(\%) = \frac{\rho_c}{\rho}\left(\frac{\rho - \rho_a}{\rho_c - \rho_a}\right) \times 100 \tag{11}$$

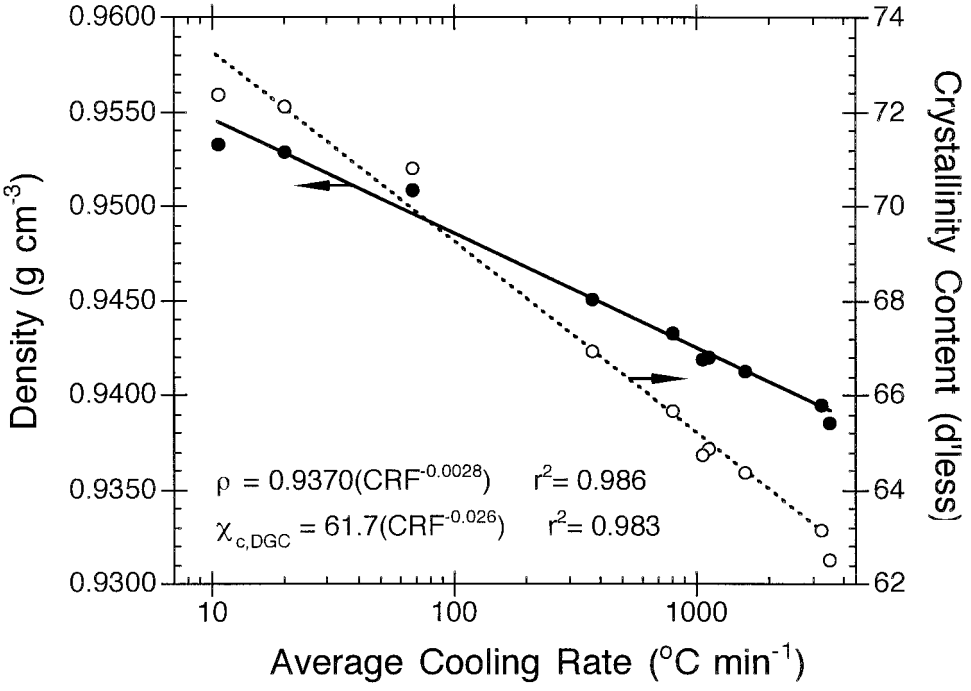

Figure 8 Overlay plots of ρ and χ_c calculated therefrom versus the ACR.

$$\chi_{c,\mathrm{DSC}}(\%) = \frac{\Delta H_f}{\Delta H_f^0} \times 100 \qquad (12)$$

where ρ, ρ_a, and ρ_c are the sample density and the densities of the pure amorphous and pure crystalline samples, respectively (i.e., for HDPE, ρ_a = 0.855 g cm^{-3} and ρ_c = 0.997 g cm^{-3} [35]), and ΔH_f and ΔH_f^o represent the enthalpies of fusion of the sample and that of the 100% crystalline sample, respectively (i.e., for HDPE, ΔH_f^o = 288 J g^{-1} [36]).

According to both figures, the density, melting peak temperature, enthalpy of fusion, and relevant apparent crystallinity content all decrease with an increasing cooling rate. This corresponds well to the general notion of polymer crystallization, which is attributable to both the thermodynamic and kinetic contributions. It is generally known that lamellar thickness is an increasing function of the crystallization temperature, as described by the Gibbs–Thomson equation,[32,33] and that the thicker the lamellae are, the higher the melting point will be. Because it has been shown earlier in Figure 2(b) that the crystallization temperature (i.e., T_p) is a decreasing function of the cooling rate, the lamellar thickness and melting peak temperature should, likewise, be a certain decreasing function of the cooling rate.

As the cooling rate increases, the rate of crystallization also increases, and the time interval during which the crystallization occurs becomes shorter. These facts suggest that the higher the cooling rate is, the lower the amount will be of crystallizable materials that will crystallize. In addition, as the cooling rate increases, the incorporation of defects, such as loose loops and dangling chain ends, into the bulk of the crystallizing materials may contribute to the decrease in the density and the enthalpy of fusion. Indeed, it is shown in Figures 8 and 9 that the density, melting peak temperature, and enthalpy of fusion exhibit a power-law relationship with the ACR. Because the apparent crystallinity content can be calculated from either the density or the enthalpy of fusion data, the apparent crystallinity content calculated from either set of data should also exhibit a power-law relationship with the ACR.

The fact that the apparent crystallinity content calculated from the density is higher than that from the enthalpy of fusion deserves further consideration. It was shown by Glotin and Mandelkern[36] on fractions of HDPE that the crystallinity content obtained from density is always higher than that from the enthalpy of fusion. They postulated that the crystallinity content calculated from the density incorporates contributions from the interfacial layer (i.e., the rigid amorphous phase), whereas that from the enthalpy of fusion does not.

CONCLUSIONS

These nonisothermal crystallization studies of HDPE based on the Ding–Spruiell technique showed that the bulk crystallization kinetics were a strong function of the cooling rate. Within the range of cooling rates studied, an increased cooling rate led to a decreasing crystallization temperature and a rapidly increasing

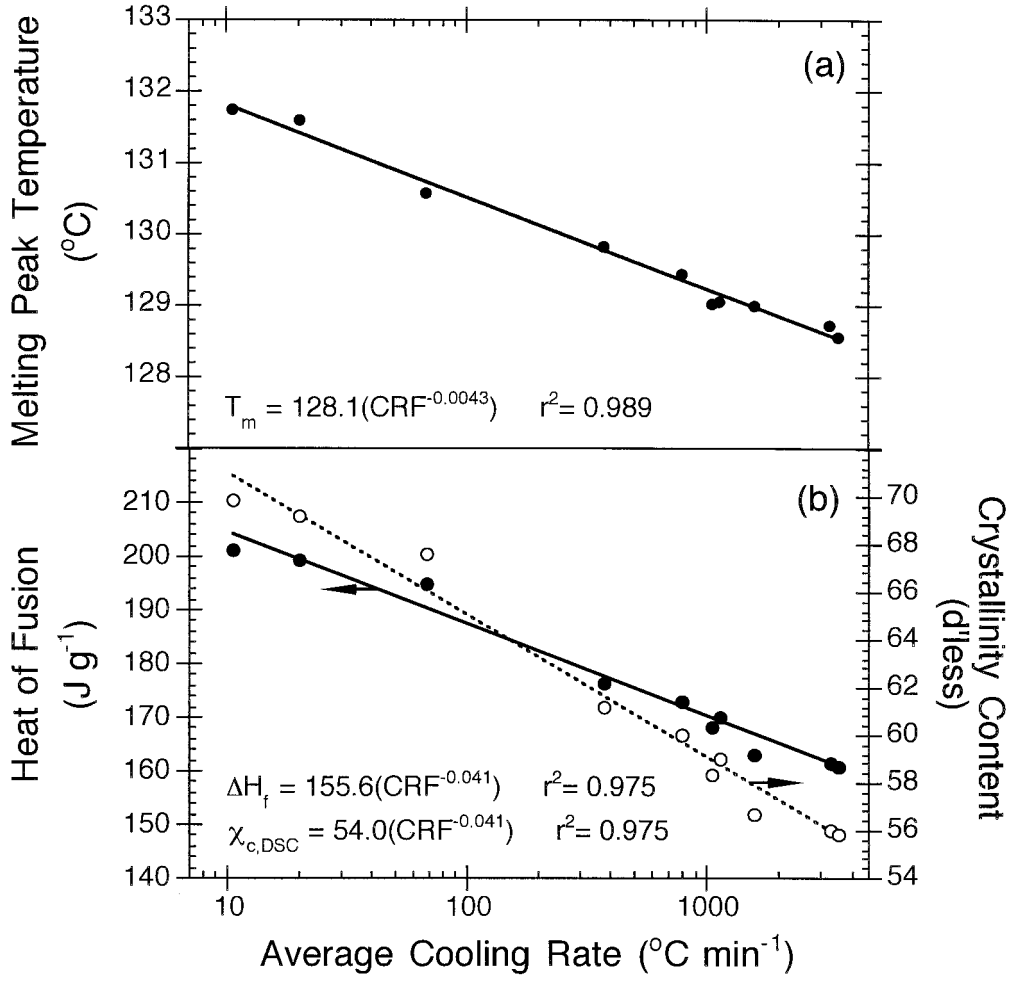

Figure 9 (a) Relationship between T_m and ACR and (b) overlay plots of ΔH_f and χ_c calculated therefrom versus the ACR.

rate of crystallization. Despite the nonisothermal nature of the technique, the bulk of crystallization took place at a pseudoisothermal temperature, a result of the competing contributions between the liberated crystallization heat and the heat carried away from the sample by the cooling medium. The technique used gave reliable, reproducible, and quantitative results under conditions that could not previously be studied by simple, traditional techniques.

The physical information, such as the density, melting peak temperature, and enthalpy of fusion, obtained from the combination of the DGC and DSC techniques exhibited a significant dependence on the cooling conditions of the samples, in that they were all found to decrease with an increasing cooling rate. A similar relation was also found with the apparent crystallinity content calculated from either the density or enthalpy of fusion data. It was postulated that, as the cooling rate increased, the decrease in the lamellar thickness and the incorporation of defects, such as loose loops and dangling chain ends, into the bulk of the crystallizing materials were the main contributions to such phenomena.

P. Supaphol acknowledges a grant provided by Chulalongkorn University through Development Grants for New Faculty/Researchers.

References

1. Di Lorenzo, M. L.; Silvestre, C. Prog Polym Sci 1999, 24, 917.
2. Janeschitz-Kriegl, H.; Wippel, H.; Paulik, C.; Eder, G. Colloid Polym Sci 1993, 271, 1107.
3. Wu, C.-H.; Eder, G.; Janeschitz-Kriegl, H. Colloid Polym Sci 1993, 271, 1116.
4. Ding, Z.; Spruiell, J. E. Soc Plast Eng Annu Tech Conf Proc 1994, 1485.
5. Ding, Z.; Spruiell, J. E. J Polym Sci Part B: Polym Phys 1996, 34, 2783.
6. Magill, J. H. Polymer 1961, 2, 221.
7. Magill, J. H. Polymer 1962, 3, 35.
8. Kim, Y.-C.; Kim, C.-Y.; Kim, S.-C. Polym Eng Sci 1991, 31, 1009.
9. Supaphol, P. M.S. Thesis, University of Tennessee, 1996.
10. Supaphol, P.; Phillips, P. J.; Spruiell, J. E. Soc Plast Eng Annu Tech Conf Proc 1997, 1546.
11. Supaphol, P.; Spruiell, J. E. J Polym Sci Part B: Polym Phys 1998, 36, 681.
12. Wagner, J.; Abu-Iqyas, S.; Monar, K.; Phillips, P. J. Polymer 1999, 40, 4717.
13. Kolmogorov, A. N. Izv Akad Nauk Ser Math 1937, 1, 355.

14. Johnson, W. A.; Mehl, K. F. Trans Am Inst Min Metall Eng 1939, 135, 416.
15. Avrami, M. J Chem Phys 1939, 7, 1103.
16. Avrami, M. J Chem Phys 1940, 8, 212.
17. Avrami, M. J Chem Phys 1941, 9, 177.
18. Evans, U. R. Trans Faraday Soc 1945, 41, 365.
19. Supaphol, P.; Spruiell, J. E. J Macromol Sci Phys 2000, 39, 257.
20. Incropera, F. P.; DeWitt, D. P. Fundamentals of Heat and Mass Transfer, 3rd ed.; Wiley: New York, 1990.
21. Banks, W.; Sharples, A.; Hay, J. N. J Polym Sci Part A: Gen Pap 1964, 2, 4059.
22. Tobin, M. C. J Polym Sci Polym Phys Ed 1974, 12, 399.
23. Tobin, M. C. J Polym Sci Polym Phys Ed 1976, 14, 2253.
24. Tobin, M. C. J Polym Sci Polym Phys Ed 1977, 15, 2269.
25. Malkin, A. Y.; Beghishev, V. P.; Keapin, I. A.; Bolgov, S. A. Polym Eng Sci 1984, 24, 1396.
26. Urbanovici, E.; Segal, E. Thermochim Acta 1990, 171, 87.
27. Wunderlich, B. Macromolecular Physics; Academic: New York, 1976; Vol. 2, p 132.
28. Kim, M.-H. Ph.D. Dissertation, University of Tennessee, 1996.
29. Wust, C. Ph.D. Dissertation, University of Tennessee, 1982.
30. Price, F. P. In Nucleation; Zettlemoyer, A. C., Ed.; Marcel Dekker: New York, 1969; Chapter 8.
31. Wunderlich, B. Macromolecular Physics; Academic: New York, 1976; Vol. 2, Chapter 5.
32. Hoffman, J. D.; Davis, G. T.; Lauritzen, J. I., Jr. In Treatise on Solid State Chemistry; Hannay, N. B., Ed.; Plenum: New York, 1976; Vol. 3, Chapter 7.
33. Hoffman, J. D.; Miller, R. L. Polymer 1997, 38, 3151.
34. Phillips, P. J.; Lambert, W. S. Macromolecules 1990, 23, 2075.
35. Brandrup, J.; Immergut, E. H. Polymer Handbook; Wiley: New York, 1989; p V15.
36. Glotin, M.; Mandelkern, L. Colloid Polym Sci 1982, 260, 182.